Nonlinear Optical Absorption and Induced Thermal Scattering Studies in Organic and Inorganic Nanostructures

V. Sai Muthukumar[1], Ramakrishna Podila[2], Benoy Anand[1], S. Siva Sankara Sai[1], K. Venkataramaniah[1], Reji Philip[3] and Apparao M. Rao[2,4]
[1]Department of Physics, Sri Sathya Sai Institute of Higher Learning, Vidyagiri, Puttaparthi, Andhra Pradesh, India
[2]Department of Physics and Astronomy, Clemson University, Clemson, SC, USA
[3]Light and Matter Physics Group, Raman Research Institute, Bangalore, India
[4]Center for Optical Materials Science and Engineering Technologies, Clemson University, Clemson, SC, USA

Definition

Nonlinear optics (NLO) studies the behavior of light in *nonlinear media*, whose dielectric polarization (***P***) responds nonlinearly to the electric field (***E***) of the light. In general, such nonlinear behavior is observed under highly intense light beams. Several fundamental properties of materials such as nonlinear absorption, nonlinear refraction, harmonic generation, etc., can be probed using NLO spectroscopy.

The field of nonlinear optics (NLO) emerged into prominence more than three decades ago with the development of the laser. These milestone discoveries have not only generated much interest in laser science but also set the stage for future work in nonlinear optics. In recent years, the discovery of various nanoscale materials such as fullerenes, carbon nanotubes, and metallic and other semiconducting nanostructures has allowed nonlinear spectroscopy to progress towards technological applications, and the focus has been on the discovery of materials with higher photonic functionalities and better performance [1, 2]. Knowledge of electronic transitions is essential in understanding the linear and nonlinear optical properties of nanomaterials. Many spectroscopic techniques such as optical absorption, photoluminescence, photoacoustics, and x-ray photoelectron spectroscopy are often employed for the investigation of energy levels in nanostructures. More significantly, estimation of the nonlinear interaction of light with nanostructures helps one to probe the higher electronic levels, which are not easily accessible otherwise.

In nanostructures, quantum confinement effects and surface plasmon resonance (SPR), in tandem with other crucial factors like morphology, particle size, and chemical environment, can lead to interesting changes in nonlinear properties with many promising applications such as ultrafast optical switching, optical limiting, passive mode locking, frequency up-conversion lasing, optical data storage, multiphoton-based laser microscopy, etc. Interestingly, various nanomaterials exhibit distinct intensity-dependent nonlinear responses for laser excitation that depends on parameters such as laser wavelength, pulse duration, and repetition rate [2]. The physical basis of observed nonlinear optical responses in nanostructures is briefly elucidated in the

In: Bhushan, B. (Ed.)Encyclopedia of Nanotechnology. Springer, Dordrecht. 2016
https://doi.org/10.1007/978-94-017-9780-1_63

following sections along with an outline for various experimental techniques used for probing their photophysical properties with special reference to the optical limiting application. Optical limiters are materials which are transparent at lower incident fluences, but attenuate light considerably at higher fluences; thus protecting eye and photosensors from damage due to intense optical sources. Various nanostructures are promising as efficient and broadband optical limiters when compared to conventional materials like organic chromophores and dyes [1, 2]

Nonlinear Optical Processes

In general, the response of a material medium (which is lossless and dispersionless) to input light can be described in terms of the electric polarization $\boldsymbol{P}$ [1], which is usually expanded in a Taylor series in the electric field amplitude $\boldsymbol{E}$ as

$$\boldsymbol{P}=\chi^{(1)}\boldsymbol{E}+\chi^{(2)}\boldsymbol{EE}+\chi^{(3)}\boldsymbol{EEE} \tag{1}$$

where $\boldsymbol{\chi^{(n)}}$ are the susceptibility tensors of order n. Far away from a material resonance, the susceptibilities are predominantly real and the material response is instantaneous, but as resonances are approached, the susceptibilities will become complex, with relatively slower responses. The first term, $\boldsymbol{\chi^{(1)}}$, is responsible for linear absorption and refraction, while the remaining terms are associated with different light-induced nonlinear effects. Second-order nonlinear effects due to $\boldsymbol{\chi^{(2)}}$ are present only in noncentrosymmetric materials, and these include second harmonic generation and other three-wave mixing processes, optical rectification, and the electro-optic Pockels effect. Nonlinear optical effects involving the third-order susceptibility $\boldsymbol{\chi^{(3)}}$ include phenomena such as third harmonic generation and four-wave mixing processes, the electro-optic Kerr effect, two-photon absorption, and Raman amplification.

For a nonlinear optical medium, the refractive index and absorption coefficient will be functions of the incident light intensity. For an isotropic centrosymmetric material (where the lowest order nonlinearity is cubic), the intensity-dependent nonlinear refractive index is given by [1–4]

$$n = n_0 + n_2 I \tag{2}$$

and the intensity-dependent nonlinear absorption coefficient is given by

$$\alpha = \alpha_0 + \beta I \tag{3}$$

where n_2 is the nonlinear refractive index coefficient, and β is the nonlinear absorption coefficient. n_0 and α_0 are the linear refractive index and linear absorption coefficient, respectively. I is the intensity of the incident light which is proportional to $\boldsymbol{E}^2$. The third-order nonlinear susceptibility can be very generally written as

$$\chi^{(3)} = \chi^{(3)}_{(R)} + \chi^{(3)}_{I} \tag{4}$$

where the real part $\chi^{(3)}_{(R)}$ accounts for effects that are transient and consume no energy (like the optical Kerr effect, molecular orientation, electrostriction, etc.). The imaginary part $\chi^{(3)}_{I}$ accounts for processes that involve losses such as two-photon absorption. Thus, $\chi^{(3)}$ (both the real and imaginary parts) serves as a figure of merit for investigating potential novel materials for photonic applications.

It may be noted that ultrafast laser pulse excitation (typically in the femtoseconds regime) provides a way to measure pure-electronic nonlinearities exclusively. To observe longer timescale processes such as excited state absorption and thermal lensing, longer laser pulses (typically in the nanosecond regime) are used.

Nonlinear Refraction (NLR)

The dominant physical mechanism driving nonlinear refraction in a given medium can vary depending on the material, optical wavelength, irradiance, timescale of the light-matter interaction, and/or geometry. In addition to bound electronic nonlinearities, which are instantaneous, effects like intramolecular motion, molecular reorientation, electrostriction, induced population

change, and photothermal effects may become responsible for nonlinear refractive index in a medium. Depending on the sign (positive or negative) and magnitude of the value of "n_2" in Eq. 2, a laser beam passing through the nonlinear medium may be self-focused or defocused. Such focusing (or defocusing) arising from the real part of the third-order nonlinear susceptibility ($\chi^{(3)}_{(R)}$) is known as the optical Kerr effect (Kerr lens effect). The instantaneous nature of Kerr lensing is used in several applications including optical switching and laser mode-locking, especially in the ultrafast regime. At very high intensities, the optical Kerr effect may tend to saturate. For relatively shorter optical pulses with very high intensity, electronic nonlinearities may, on the other hand, lead to self-steepening and supercontinuum generation effects.

Nonlinear refraction can also occur due to thermal effects (usually referred to as thermal lensing), which typically build up with a relatively long response time of a few milliseconds. Thermal nonlinearity can be dominant for continuous-wave (CW) laser excitation and significant for nanosecond laser pulse excitation. The variation of the refractive index with temperature can be described mathematically as $\tilde{n} = n_o + (dn/dT)\tilde{T}_0$, where n_o is the linear refractive index, $\tilde{T}_0$ is the laser-induced change in temperature, and dn/dT, the temperature-dependent refractive index. The thermal nonlinear index of refraction can be determined using a closed aperture Z-scan measurement, employing either the thermal lens model (TLM) or Sheik-Bahae's formalism [3] for analysis.

Nonlinear Absorption

Nonlinear absorption refers to the change in the transmittance of a material as a function of input light fluence (given in units of J/m^2) [1]. As given above, the nonlinear absorption coefficient of a third-order nonlinear medium can be written as $\alpha = \alpha_0 + \beta I$, where β is the nonlinear coefficient of absorption. Far away from a material resonance, β usually reduces to the two-photon absorption coefficient. However, near a material resonance, two-step phenomena like excited state absorption (ESA) and free carrier absorption (FCA) may also contribute to nonlinear absorption. Such phenomena are collectively referred to as reverse saturable absorption (RSA). An overview of these phenomena is given below.

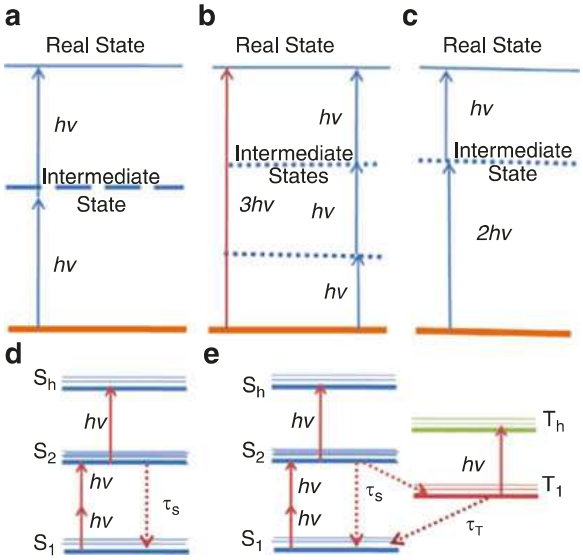

Nonlinear Optical Absorption and Induced Thermal Scattering Studies in Organic and Inorganic Nanostructures, Fig. 1 Various nonlinear absorption schemes involving 2PA, 3PA and ESA processes. (**a**) depicts an ESA process while (**b**) shows 3PA and (**c**) shows 2PA. The dotted lines represent virtual state and *solid lines* represent real state. (**d**) and (**e**) show three- and five- level ESA models respectively, which have been extensively used in literature (see Ref. [1] for details). (**a**) 2PA virtual intermediate state (*dashed line*). (**b**) 3PA virtual intermediate state (*dotted line*). (**c**) ESA real intermediate state (*dotted line*)

Multiphoton Absorption

Many semiconducting and metallic nanomaterials exhibit multiphoton absorption (MPA). In this discussion, MPA is limited to two- and three-photon absorption (2PA and 3PA, respectively) processes. 2PA involves the simultaneous absorption of two photons to promote an electron from an initial state to a final state through a virtual intermediate level (Fig. 1). 3PA has a lower transition probability and involves three photons and two intermediate states. Since the intermediate level is virtual, energy need be conserved only in the final state. In contrast to reverse saturable absorption, MPA is an instantaneous process occurring in femtosecond timescales. The mechanism of 2PA can be viewed as analogous to a

three-level RSA process where the lifetime of the intermediate state approaches zero and the ground state absorption is extremely low (high linear transparency). Two- and three-photon-absorption-based nanomaterials can be used for applications like frequency conversion lasing, optical limiting, pulse stabilization, and reshaping [1].

Excited State Absorption

In systems like C_{60}, the excited state absorption (ESA) cross section is greater than the ground state absorption cross section, which can lead to an enhanced absorption at higher input intensities. Typically, the ESA process is much stronger than 2PA, and to indicate the collective contribution of 2PA and ESA, the term "effective 2PA" is sometimes used in literature. When excited with nanosecond laser pulses, which are relatively long compared to typical excited state lifetimes of nonfluorescent materials, ESA will contribute significantly to nonlinear absorption. For instance, the effective 2PA cross section of a medium measured under nanosecond (ns) pulse excitation has been found to be about two orders of magnitude larger than the intrinsic 2PA cross section measured under femtosecond (fs) excitation [5]. In the case of intrinsic 2PA, the nonlinear absorption coefficient (β) is independent of the input intensity, but in the case of effective 2PA, the nonlinear absorption coefficient (β_{eff}) varies with input intensity. Relevant examples are discussed in section "Experimental Methods". Another interesting case is that of TPA-induced ESA, where a strong 2PA process considerably increases molecular populations in an excited state, which then absorbs another photon by an ESA process.

Free Carrier Absorption

In semiconducting materials, charge carriers are generated by one-photon as well as two-photon excitations. These electrons or holes can be excited to still higher or lower states in the conduction or valence bands by absorbing additional photons. Such carrier-assisted nonlinear absorption processes are known as "free carrier absorption," which is analogous to excited state absorption in molecular systems [2]. One difference is that free carrier absorption processes are usually independent of the input laser pulse width (assuming shorter timescales for carrier diffusion and recombination). In addition, they are insensitive to particle size and geometry and can be found in both solids and nanoparticle dispersions covering a broad range of temporal and wavelength ranges.

Induced Thermal Scattering

An important mechanism by which laser light transmitted through a medium suffers losses, particularly in the nanosecond excitation regime, is induced thermal scattering (ITS). Processes including the formation of microplasma and solvent microbubbles, and thermally induced local refractive index gradients lead to ITS [4]. Since the formation of thermal scattering centers takes several nanoseconds, these phenomena generally do not affect the transmission of ultrafast laser pulses through the medium. Mechanistically, ITS leads to a spatial redistribution of the incident beam (as shown in Fig. 2), resulting in spatial intensity modulation, which can be efficiently used for optical limiting if appropriate geometries are employed [2, 4].

Experimental Methods

In order to evaluate the contribution of various intensity-dependent nonlinear processes in any material, different methods such as second harmonic generation, four-wave mixing, ellipse rotation, nonlinear interferometry, and Z-scan are often employed [1, 2]. In recent years, Z-scan and four-wave mixing methods have been extensively adopted and applied by various research groups across the world to evaluate the nonlinear optical properties of various bulk and nanostructured materials.

Four-Wave Mixing

Four-wave mixing (FWM) is a phase-sensitive nonlinear effect arising from third-order optical nonlinearity. The concept of three optical fields interacting to produce a fourth optical field is central to the description of all four-wave mixing processes. Along with Z-scan, this is one of the

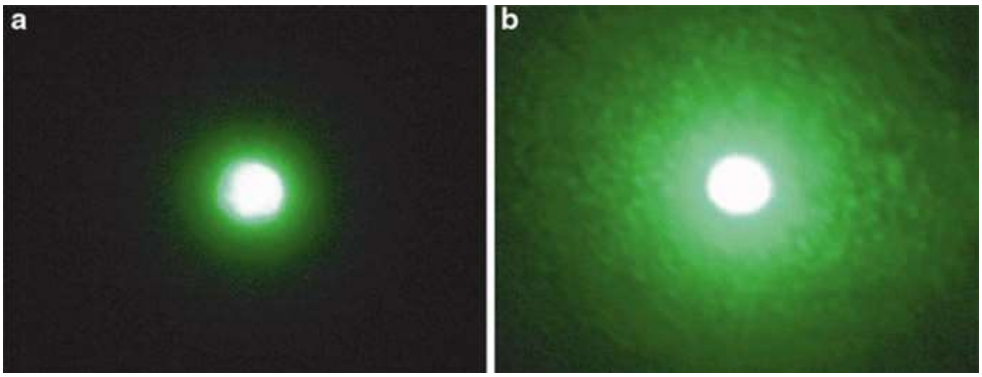

Nonlinear Optical Absorption and Induced Thermal Scattering Studies in Organic and Inorganic Nanostructures, Fig. 2 Panel (**a**) shows the transverse profile of the incident laser beam, while panel (**b**) shows the beam profile of the scattered beam after traversing through the sample [6]

most widely used techniques to measure the third-order susceptibility $\chi^{(3)}$ of materials [2, 3]. In a dielectric medium, when two light beams are present, each beam independently polarizes the dielectric. The interference between polarized fields then results in harmonics at the sum and difference frequencies. When a third field is incident on the dielectric, it too drives the polarization and will beat with both the other input fields as well as the sum and difference frequencies. This beating with the sum and difference frequencies gives rise to the fourth field in four-wave mixing.

The FWM process is essentially of two types: nondegenerate and degenerate (DFWM). In the former, the optical excitation sources are of different wavelengths, while in the latter, their wavelengths are identical. The strength of the fourth beam is dependent on a coupling constant that is proportional to the effective $\chi^{(3)}$, and hence, measurement of the observed signal will yield information about the $\chi^{(3)}$ tensor components of the medium. Furthermore, DFWM can be employed in the backward (phase conjugate) and BOXCARS configurations, with the choice being made through consideration of the experimental conditions and requirements. In the backward geometry, two waves travel in the backward direction and two travel in the forward direction, whereas in the BOXCARS geometry, all the four waves travel in the forward direction. Using different polarizations for the three beams, all the components of the $\chi^{(3)}$ tensor can be measured. In terms of the intensity-dependent refractive index, the DFWM process is considered to be the interference of two input beams leading to a spatial periodicity resulting in the formation of a grating from which the third beam scatters, generating the fourth wave.

FWM can be used to probe either one-photon resonances or two-photon resonances in a material by measuring the resonant enhancement as one or more of the frequencies are tuned. By tuning the frequencies to multiple resonances in the material, excited state cross sections, lifetimes, and line widths can be measured. One of the main disadvantages of FWM is its sensitivity to alignment, requiring all three coherent beams to simultaneously overlap within the sample in space and time.

Z-Scan

The Z-scan technique is a sensitive and simple method employed to measure nonlinear absorption and nonlinear refraction. It has been used extensively to study the optical nonlinearity of various materials like semiconductors, nanocrystals, semiconductor-doped glasses, liquid crystals, organic materials, and biomaterials. Introduced by Sheik-Bahae et al. [3] in the early 1990s, this widely used technique has many advantages over other nonlinear spectroscopic methods. In a typical Z-scan, the light-induced change in transmittance (ΔT) of a medium due to optical nonlinearity is measured as a function of input light energy density (fluence) or intensity. A continuous variation of the input fluence is

achieved by translating the sample under study through the focal region of a focused laser beam (the sample position is taken as z with $z = 0$ being the focal point for the incident laser beam, hence the name "*Z*-scan"). Consequent increase and decrease of the intensity incident at the sample position lead to wave front distortions (created by nonlinear optical effects in the sample). There are two types of Z-scan techniques, namely, the "closed aperture" Z-scan and the "open aperture" Z-scan.

In the closed aperture Z-scan, which is used for studying nonlinear refraction (NLR), the transmitted beam is passed through an aperture placed in the far field and then measured by a detector, for different values of sample position z. When the medium is far before the focal plane, no self-lensing occurs. As the medium approaches the focal plane, the high intensity begins to induce a lensing effect in the medium. For a negative nonlinearity, this lens tends to collimate the beam, thereby increasing the transmittance through the aperture. At the focal plane, even though the intensity is highest, the influence of the induced lens is minimized, resulting in a transmittance comparable to the linear transmittance. This is similar to placing a thin lens at the focus of a beam; this results in a minimal effect on the far field beam pattern. As the sample is translated beyond the focal plane, the negative lens tends to increase the beam divergence, resulting in a decrease in the aperture transmittance. As the medium is translated still farther from focus, the intensity again becomes weak enough that the induced lensing is negligible. This sequence results in a change in transmittance with a characteristic peak followed by a valley, which is symmetric about the focal plane ($z = 0$). For a positive nonlinearity, the pattern consists of a valley followed by a peak. Thus, a simple Z-scan experiment can give both the sign and magnitude of the optical nonlinearity in a material. In both these cases, a purely refractive nonlinearity is considered, assuming that no absorptive nonlinearities are present. The sensitivity to nonlinear refraction results from the vital role played by aperture A (Fig. 3). If aperture A is removed, then the *Z*-scan is sensitive only to nonlinear absorption (NLA), and this configuration is commonly referred to as the open aperture Z-scan. The absorptive nonlinearity will be a maximum at the focal plane, where the intensity is highest. Thus, the open aperture scheme is employed to characterize materials that exhibit NLA, such as excited state absorption (ESA), two-photon absorption (TPA), saturable absorption (SA), etc.

Even though closed aperture Z-scan is used to study only NLR, in practice, the closed aperture Z-scan curve may contain a contribution from NLA also, depending on the sample. To obtain the NLR coefficient in such a case, it is sufficient to normalize the closed aperture data using the open aperture data before analysis. Although the open aperture Z-scan technique is adequate to detect the presence of nonlinear absorptive effects, it cannot singularly identify the nature of an absorptive nonlinearity. For example, at the outset, it cannot differentiate a 2PA signature from a two-step excitation signature. Figure 4 shows typical Z-scan curves simulated for the MPA, SA, and RSA processes. The Z-scan curves for SA (peak) and RSA (valley) have shapes, which are complementary to each other. It should be noted that the Z-scan curves for RSA and MPA

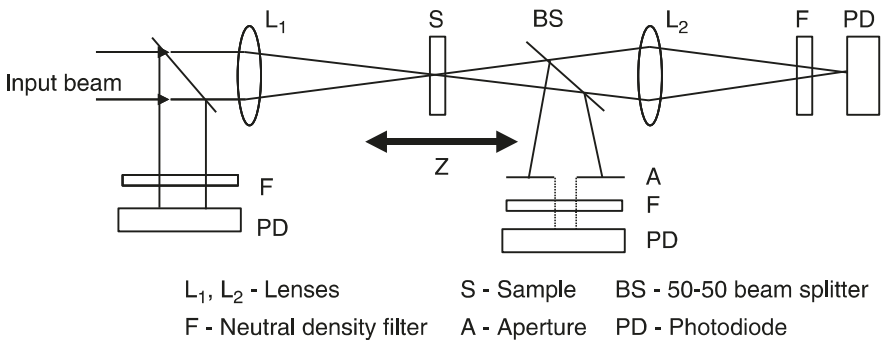

Nonlinear Optical Absorption and Induced Thermal Scattering Studies in Organic and Inorganic Nanostructures, Fig. 3 A conventional Z-scan layout for simultaneous open aperture and closed aperture measurement

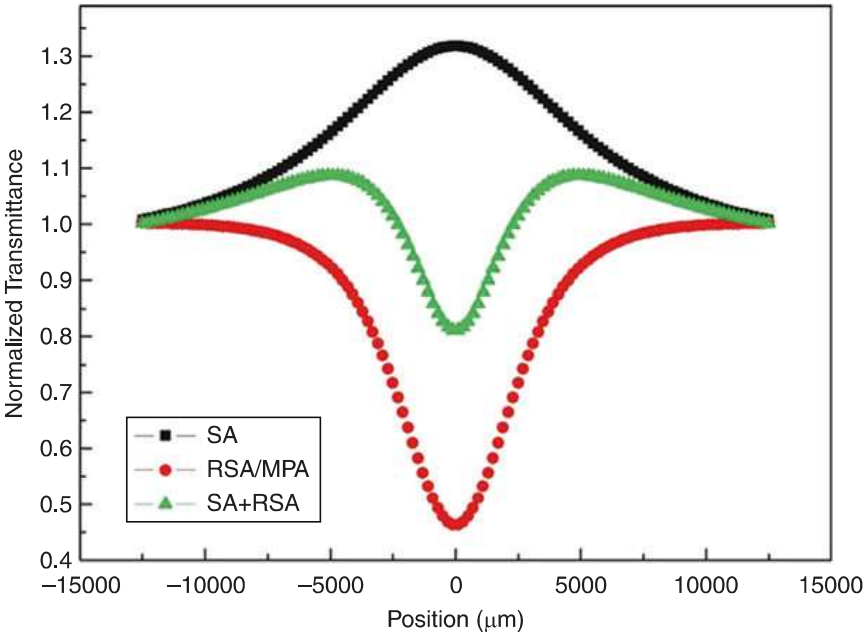

Nonlinear Optical Absorption and Induced Thermal Scattering Studies in Organic and Inorganic Nanostructures,
Fig. 4 Simulated Z-scan curves for the saturable absorption (*SA*), reverse saturable absorption (*RSA*), and multiphoton absorption (*MPA*) processes

look very similar to each other. To confirm the exact nature of the process, it is often necessary to know the linear absorption properties of the sample from a linear absorption spectrum taken using a spectrophotometer. Z-scans performed using ultrafast laser pulses (where RSA effects are a minimum) will also be instructive in this regard.

A recent variation in the Z-scan technique is the white-light continuum Z-scan, where a supercontinuum is used as the light source for doing the Z-scan experiment. The "supercontinuum" is an intense, ultrafast, broadband light pulse, with wavelengths spanning the UV to the near IR region, generated when an ultrafast laser pulse is passed through certain transparent NLO media like heavy water. Conversion of the spectrally narrow pump pulse into the resultant broad spectrum involves the interplay of self-phase modulation and self-focusing of the pulse, due to an intensity-dependent refractive index of the medium. Since the typical supercontinuum spectrum covers the whole visible range, it appears white, and hence it is also known as a "white-light continuum." In the conventional Z-scan technique, nonlinearity can be measured only for one wavelength in one measurement. To determine the spectral dispersion of the nonlinearity, a tunable laser source has to be used, and separate Z-scans need to be done at all the required wavelengths. Obviously, this approach is time consuming and tedious. The idea of using a strong white-light continuum (WLC) as the light source to measure the dispersion of the nonlinearity in a single Z-scan experiment was therefore proposed by Van Stryland's group [7]. Their "WLC Z-scan" allows for rapid, broadband characterization of degenerate NLA and NLR.

Nonlinear Optical Properties of Nanomaterials

Nonlinear optical measurements in low-dimensional materials continue to draw considerable attention since the nonlinear behavior of the complex refractive indices lead to unique optical phenomena [1–3, 7]. Furthermore, the quantum confined nature of the charge carriers, surface effects, and sharp density of states in low-dimensional materials such as nanoparticles, nanowires, nanotubes, and nanorods introduces various new fundamental physical phenomena that can influence the NLO properties. For example, surface effects can lead to ferromagnetic behavior in nanostructured ZnO whereas bulk ZnO is diamagnetic [8], and a semimetal to semiconductor transition occurs in the low dimensional

Nonlinear Optical Absorption and Induced Thermal Scattering Studies in Organic and Inorganic Nanostructures, Table 1 Different nonlinear optical processes observed in different nanostructured materials (see text for details)

Type of nanostructures	Cause for NLO properties	Technique used for probing	Reference
C60 Dispersions	NLA (2PA)	Pump-probe techniques	Tutt et al. [4]
	NLR, RSA, NLS, thermal NLO	Z-scan	
C60 Films	NLR, NLA(SA)	Z-scan	
SWNT films	NLR, NLA (FCA)	Z-scan, pump-probe techniques	Chin et al. [9]
SWNTs suspensions	NLR, NLS	Z-scan	
MWNT suspension	NLS	Z-scan and optical limiting measurements	
Metal nanowires	NLS	Optical limiting measurement	Pan et al. [10]
Gold nanoparticles dispersions	NLA, NLS	Z-scan and optical limiting measurements	Reji Philip et al. [11]
CdSe-based quantum dots suspensions	NLR, NLA	Z-scan and optical limiting measurements	Ganeev et al. [12]

forms of bismuth due to quantum confinement effects. Hence, one may utilize these interesting properties of nanostructures to tailor new materials for NLO applications. For example, optical switching, saturable absorption, and optical limiting properties of one-dimensional nanostructures have shown considerable promise compared to bulk materials. In this section, several interesting NLO phenomena which can be observed in various nanostructures using the *Z*-scan technique are discussed. Although the discussion is limited to the *Z*-scan technique, various experimental techniques used for probing the NLO properties of popular nanostructures are summarized in Table 1.

Carbon Nanotubes

One-dimensional carbon nanotubes (CNTs) have revolutionized various fields of science and technology since their optical and electrical properties allow one to selectively modify and tailor nanotube properties for specific applications. Initial reports on the nonlinear optical limiting performance of multiwalled carbon nanotubes (MWNTs) highlighted the superior performance of nanotubes compared to corresponding properties of C_{60} and carbon black dispersions. Subsequently, it spurred interest in investigating NLO properties of functionalized CNT-based novel nanomaterials. Moreover, the broadband optical absorption profile of carbon nanotubes provides a unique advantage over other optical materials including fullerenes. Theoretical predictions by Margulis et al. claimed that the third-order nonlinear optical susceptibility for MWNTs exceeds that of fullerene molecules by two orders of magnitude [13]. Such enhancement in third-order NLO values arises from the combined effect of π-electron transitions, which are dominant over interband/intraband transitions. Thus, the modification of the π-electron cloud via functionalization or doping provides an efficient means for engineering novel materials with high nonlinear optical susceptibility.

The optical limiting performance of MWNTs at 532-nm excitation wavelength with a 7-ns pulsewidth from a second harmonic generator of a high-power Nd:YAG system (quanta systems) is depicted in Fig. 5. The laser excitation was used in the conventional open aperture *Z*-scan setup (as described in section "Experimental Methods"). Optical limiting response was studied by varying parameters such as the solvent used for nanotube suspension and the incident energy. The MWNTs were suspended in solvents such as deionized water, 2-propanol, and ethanol using sonication (for about ~10 min).

The transmittance curves of MWNT suspensions, as shown in Fig. 5, at different energies indicated improved limiting at higher energies. As expected, in the case of higher energies, early onset of limiting was observed (greater width of

transmittance curve at 40 μJ). The main mechanism responsible for the observed optical response is nonlinear-induced scattering, which was evident as the MWNTs suspension translated across the focal plane in the Z-scan experiment. The observed NLO response of MWNTs arises due to "microbubble" or "microplasma" formation that leads to the observed nonlinear scattering [4].

The leading edge of the pulse is absorbed by the MWNTs and is nonradiatively transferred to the surrounding medium within a few nanoseconds, which causes thermal inhomogeneities in the suspension centered around the nanotubes. Depending on the fluence (F_o) and thermo-optic coefficient (dn/dT), a local change in the temperature results in a local refractive index gradient (Δn) since $\Delta n = (dn/dT)(F0\ \alpha/2\rho C_v)$, where α is absorption coefficient, ρ is the density, and C_v is the specific heat of the sample [14]. The trailing edge of the optical pulse, therefore, "sees" a nonuniform optical medium of scatterers created by the leading edge of the pulse. Thus, the trailing edge gets scattered leading to a spatial redistribution of pulse energy (as shown in Fig. 6)

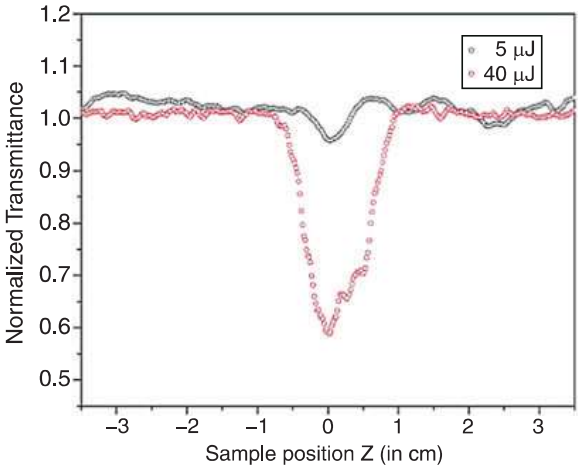

Nonlinear Optical Absorption and Induced Thermal Scattering Studies in Organic and Inorganic Nanostructures, Fig. 5 Open aperture Z-scan signal for MWNTs suspensions dispersed in water and excited at two different incident energies, 5 μJ and 40 μJ; $\lambda_{excitation} = 532$ nm

Since the thermodynamical parameters of the solvent media surrounding the nanotubes play a crucial role in the formation of a scattering center, the optical limiting response was also found to be solvent dependent [9]. The threshold fluence for optical limiting (at which the transmittance falls to 50 % its initial value) for MWNTs was determined to be ~0.5 J cm^{-2} (Fig. 7).

Bi Nanorods

Bismuth is a semimetal in its bulk form and can be prepared in several different nanostructured forms, including thin films, nanowires, nanorods, and quantum dots [15]. Bi is an attractive material for studying how nanostructuring can alter the optical properties of metals. For example, because

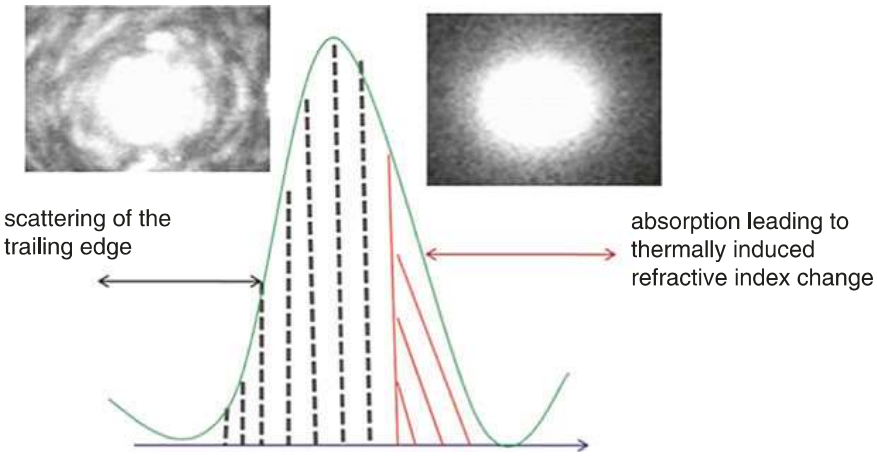

Nonlinear Optical Absorption and Induced Thermal Scattering Studies in Organic and Inorganic Nanostructures, Fig. 6 Scheme of nonlinear scattering or induced scattering leading to spatial redistribution of the beam as the intense laser pulse interacts with the MWNTs. The *right inset* shows the mm size laser spot before incidence, and the *left inset* shows the visible scattering after incidence

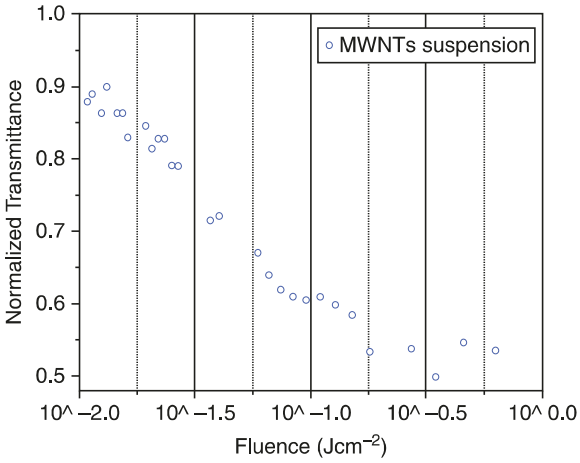

Nonlinear Optical Absorption and Induced Thermal Scattering Studies in Organic and Inorganic Nanostructures, Fig. 7 Nonlinear optical response of MWNTs suspension at 532-nm excitation

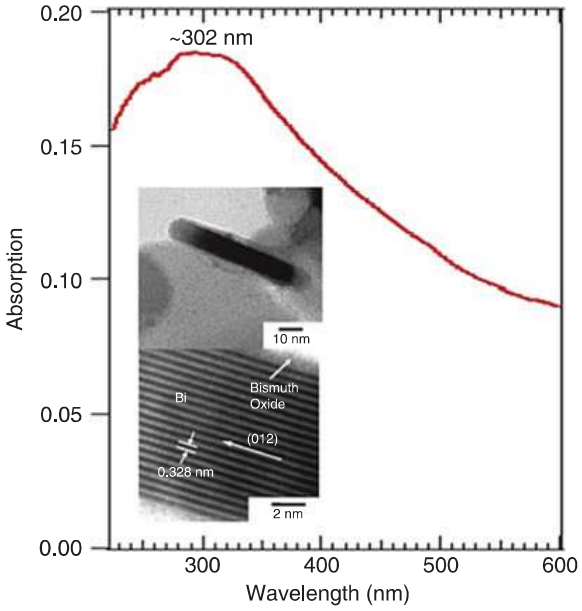

Nonlinear Optical Absorption and Induced Thermal Scattering Studies in Organic and Inorganic Nanostructures, Fig. 8 UV-Visible absorption of Bi nanorod suspension in the range of 200–600 nm. The broad peak at 302 nm is due to surface plasmons. TEM images of isolated Bi nanorods encased inside a thin oxide layer (*top inset*) and the crystalline planes (012) of trigonal Bi (*bottom inset*)

of the small effective mass components (in the anisotropic effective mass tensor) of Bi, quantum confinement effects are observed in nanowires with diameters as large as 40 nm at low temperature (77 K) [15]. In addition, since the mean free path is long in bismuth (~250 nm at room temperature), the finite size effects in a Bi crystal are more pronounced. These effects, which are observed in the tens of nanometers range in Bi, occur in other metals only at much smaller length scales and, thus, are likely to be more difficult to probe experimentally. Therefore, understanding these effects in bismuth can assist in the prediction of the optical properties of other nanostructured materials.

A semimetal to semiconductor transition was predicted in the low-dimensional forms of bismuth due to quantum confinement effects. When such a transition occurs, it is expected that several material properties undergo a radical change. For example, the thermoelectric figure of merit is poor in bulk Bi due to nearly equal and opposite contributions from electrons and holes, but is high, ~2, in small-diameter Bi nanowires. Similar enhancements in NLO properties were also observed for Bi nanorods [16].

Figure 8 shows the transmission electron microscope (TEM) images for Bi NRs synthesized using pulsed vaporization techniques [16]. Unlike bulk Bi, bismuth nanoparticles and nanorods exhibit a broad surface plasmon (SP) peak at ~281 and ~302 nm (4.4 and 4.1 eV), respectively. When irradiated by 532 nm (2.33 eV) laser pulses (pulse width ~7 ns), Bi NRs can absorb energy via interband and intraband transitions, free carrier absorption, and two-photon excitation. The presence of the SP peak makes the absorption a "near-resonant" process. When Bi NRs are suspended in any solvent, the absorbed energy is transferred to the surrounding medium through nonradiative de-excitation, resulting in localized heating and thus scattering centers. In the case of a Z-scan experiment, the leading edge of the pulse creates these scattering centers and the trailing edge of the pulse gets scattered (see Fig. 6). Such a mechanism has been observed for other nanostructured systems such as SWNTs and MWNTs (see section "Carbon Nanotubes").

Previously, Sivaramakrishnan et al. used visible and IR laser pulses from a Nd:YAG laser (quanta system, 7 ns, 10 Hz), at both 532 and

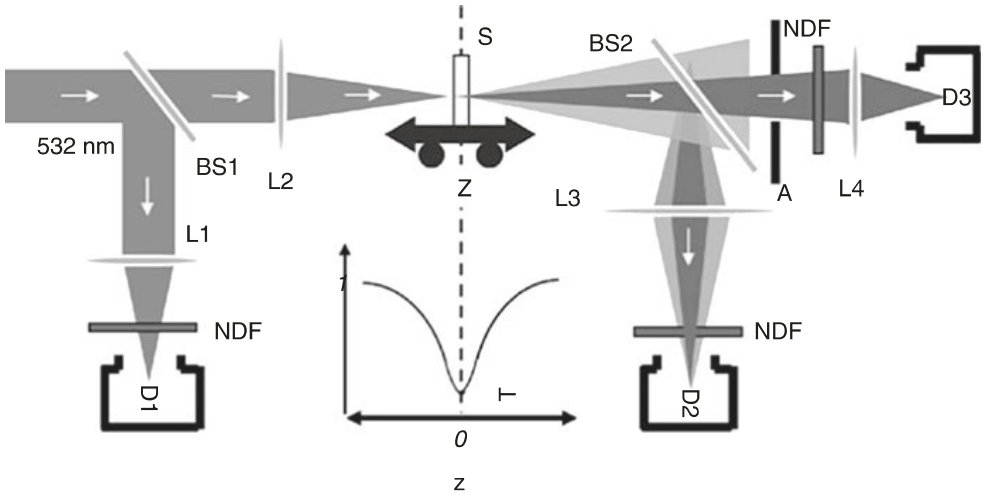

Nonlinear Optical Absorption and Induced Thermal Scattering Studies in Organic and Inorganic Nanostructures, Fig. 9 Schematic of the experimental setup used for the NLO studies of Bi nanorods. A combination of lenses (*L1–L4*), beam splitters (*BS1*) and (*BS2*), neutral density filters (*NDFs*), aperture A, and detectors (*D1–D3*) are used to measure contributions to optical limiting from the scattered and unscattered components. Bi nanorod suspension is positioned at S and translated through $z = 0$

1,064 nm, to measure the optical limiting performance of Bi nanorod suspensions by the Z-scan technique at room temperature [17]. In order to separate the contributions of NLA and NLS, a modified Z-scan setup (Fig. 9) proposed by Jourdrier et al. was employed. In the modified setup, the beam is split 50:50 (using BS2) to reach two detectors D2 and D3 in order to measure the transmittance T of the sample with detector D1 as a reference. A "2" wide lens (L4) collects light from both the scattered and unscattered parts making D2 insensitive to transmittance changes due to spatial redistribution. This ensures that the collection efficiency is ~90 %. Thus, D2 records changes in transmittance solely due to absorptive effects, and the nonlinear extinction coefficient measured by the Z-scan curve is only due to contributions from NLA. On the other hand, D3 detects only the unscattered part since aperture (A) can be adjusted to prevent the scattered part from reaching D3. Therefore, D3 records a reduced transmittance due to NLS and NLA, unlike the case of D2. The Z-scan curves for the Bi nanorods suspended in chloroform (linear optical transmittance of 60 %) in a 1-mm cuvette made of fused silica (under a 55-μJ, 532-nm, 7-ns excitation) are shown in Fig. 10.

Figure 10a shows the Z-scan curves recorded by detectors D2 (NLA alone) and D3 (NLA and NLS). The depth of the valley in the Z-scan curve is a direct measure of the extent of optical limiting and is different in the D2 and D3 curves with dips of 0.65 and 0.25, respectively. Since D2 records the contribution due to NLA alone and the D3 curve also has contributions from NLS, it is clear that NLS induced by NLA makes a significant contribution to the total extinction. In fact, the contribution of NLS to optical limiting is greater than that due to NLA. Interestingly, in the case of 1,064-nm excitation (55 μJ, 7 ns), the D2 and D3 curves overlap (Fig. 10b), and the minimum transmittance is ~0.75 in both the cases. Thus, NLS is absent at 1,064 nm, and only NLA makes a contribution to the total extinction observed at this wavelength. At 532 nm, however, both NLA and NLS are responsible for the observed optical limiting unlike the 1,064-nm case. This is very unlike the behavior of carbon black and SWNT/MWNT suspensions, where NLS dominates at both 532- and 1,064-nm excitations (see section "Carbon Nanotubes").

As shown in Fig. 8, Bi nanorods used in this study contain a native oxide layer. Z-scan experiments performed using 532-nm excitation on

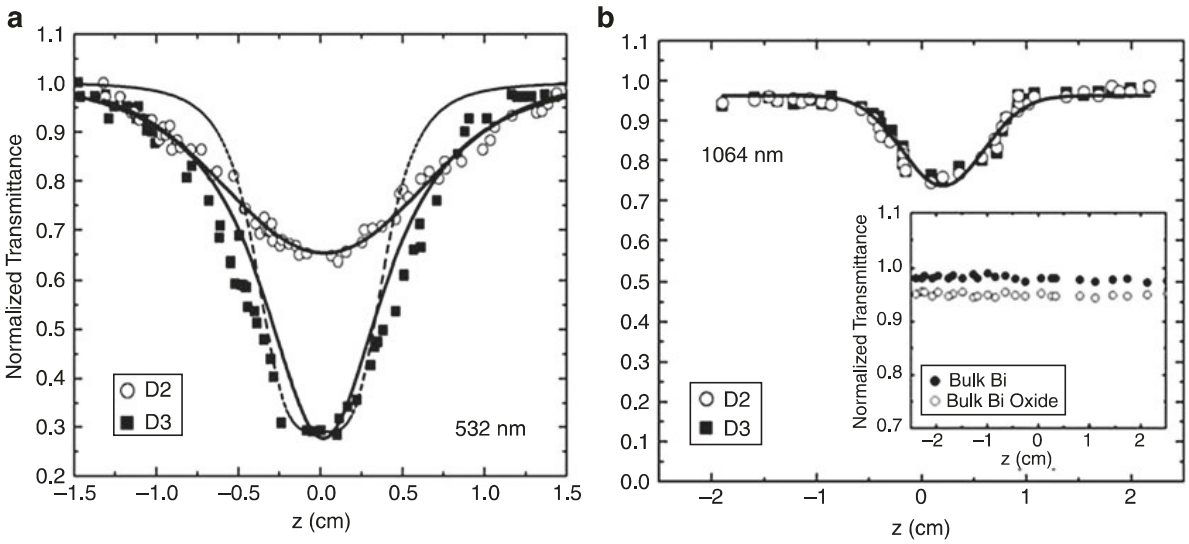

Nonlinear Optical Absorption and Induced Thermal Scattering Studies in Organic and Inorganic Nanostructures, Fig. 10 (**a**) Normalized transmittance measured at 532-nm excitation by detectors D3 (nonlinear absorption and scattering) and D2 (nonlinear absorption only) for an input energy of 55 μJ. The minimum transmittance recorded by D3 is less than that of D2 as it has contributions due to both scattering and absorption. (**b**) Same as in (**a**) using the 1,064-nm excitation for an input energy of 55 μJ. The *overlapping curves* suggest that nonlinear scattering is absent when excited with 1,064 nm in contrast to the 532-nm case

bulk Bi and bulk Bi_2O_3 did not display any nonlinearity (inset in Fig. 10b).

However, ball-milled Bi_2O_3 powder exhibited strong nonlinearity when excited at a higher fluence (90 μJ; Fig. 11a). Similar to the case of Bi nanorods, the predominant cause for such nonlinearity was found to be two-photon absorption (2PA). Additionally, the saturation of the ground state absorption was also observed for ball-milled Bi_2O_3 samples. Thus an effective nonlinear absorption coefficient $\alpha(I)$, given by $\propto (I) = \frac{\alpha_0}{1 + \frac{I}{I_S}} + \beta I$ was considered for the fitting of the data shown in Fig. 11a, where I_S is the saturation intensity (intensity at which the linear absorption drops to half its original value) and β is the 2PA coefficient. Since Bi nanorods posses a high surface area (hence more of a surface oxide layer), it is possible that the nonlinear response discussed in Fig. 10 arises from the native surface oxide layer rather than core Bi nanorods. Furthermore, in Bi_2O_3, the numerically calculated β's were found to be decreasing with increasing energy as shown in Fig. 11b. The falloff of β with increasing intensity is a consequence of reverse saturation absorption arising from a sequential 2PA [2]. Thus, the contribution of the native Bi_2O_3 layer to the nonlinear properties of Bi nanorods cannot be ruled out despite the absence of any nonlinearity in bulk forms of Bi and Bi_2O_3.

N

Surface-Modified NiS_2 Nanoparticles

Photonic nanoparticle systems have attracted considerable attention due to a wide variety of NLO applications such as optical limiting, saturable absorption, second harmonic generation, two-photon absorption, all-optical control, and holographic storage control. Typically, such systems are designed with a view of enhancing one of the nonlinear optical properties over their bulk counterparts. Previously, it was shown that nanomaterials (such as surface-modified NiS_2) can also be engineered to deliver systems displaying more complex behavior involving the interplay of two or more nonlinear phenomena [17]. If in such systems, two competing mechanisms operate simultaneously, however, the stronger dominates the weaker. Decoupling them in a single experiment is not straightforward. This section discusses the case of complete quantitative characterization in a single experiment of two *simultaneous* but *contrary* optical transmission

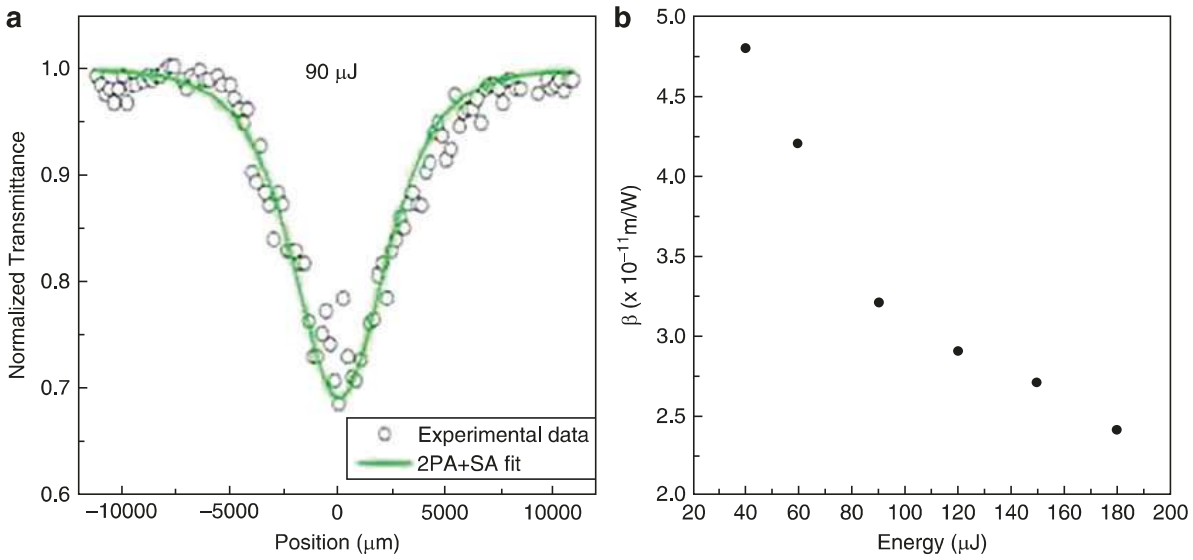

Nonlinear Optical Absorption and Induced Thermal Scattering Studies in Organic and Inorganic Nanostructures, Fig. 11 (**a**) *Z*-scan data from ball-milled Bi_2O_3 samples obtained with 532-nm, 7-ns pulses. (**b**) The variation of 2 PA coefficients as a function of incident laser energy

phenomena – optical limiting and saturable absorption in surface-modified NiS_2 nanoparticle suspensions by employing a modified *Z*-scan method as in the case of Bi nanorods (Fig. 9). Capping with dimethylglyoxime (DMG) results in the surface modification of the nanoparticles and exhibits a spectral feature essential for the saturable absorption.

NiS_2 nanoparticles were suspended in an appropriate amount of 2-propanol so that the sample held in a 1-mm-wide fused silica cuvette would have a linear transmittance of 80 % at 532-nm wavelength. The second harmonic of a Q-switched Nd: YAG laser (532 nm) of pulse width 7 ns at 10-Hz repetition was used in the *Z*-scan studies employing a converging lens with a focal length of 20 cm. The *Z-scan curve* and transmittance as a function of input fluence are shown in Fig. 12a. It is clearly evident from Fig. 12b that the optical transmittance falls as intensity increases, exhibiting an *optical limiting* behavior. A transmission of 50 % (which is the threshold fluence for optical limiting) is reached at 300 μJ/cm^2. Such optical limiting in NiS_2 occurs due to the intensity-dependent scattering that is also visible to the naked eye.

Figure 13 shows the *Z*-scan curves (with the set up shown in Fig. 9) from detectors D2 (•) and D3 (•) for NiS_2 nanoparticles suspended in 2-propanol. The *Z*-scan curve due to detector D2 (•) shows an upward *peak* indicative of the saturation of absorption. The transmittance of the sample increases as it is brought closer to the focus of the *Z*-scan lens. This is in sharp contrast to the studies on Bi nanorods discussed earlier where the corresponding curve is a *valley* indicating that nonlinear absorption increases with intensity and transmission falls with intensity (Fig. 10). Saturable absorption observed in this case is similar to the behavior of rhodamine B under similar experimental conditions [6].

Furthermore, in Fig. 13, the Z-scan curve of detector D3 (•) which records intensity-dependent transmittance due to both absorption and scattering shows a typical optical limiting valley. Closer observation reveals that both the fall in transmittance due to optical limiting (•) and the rise in transmittance (•) due to saturable absorption are at a z-position of 1.75 cm with respect to the focal point ($z = 0$). Thus, the two effects are simultaneous and not sequential as has been observed in other experiments on nanoparticles systems [18]. The sequential occurrence of saturable absorption followed by an optical limiting behavior is indicative of excited state absorption.

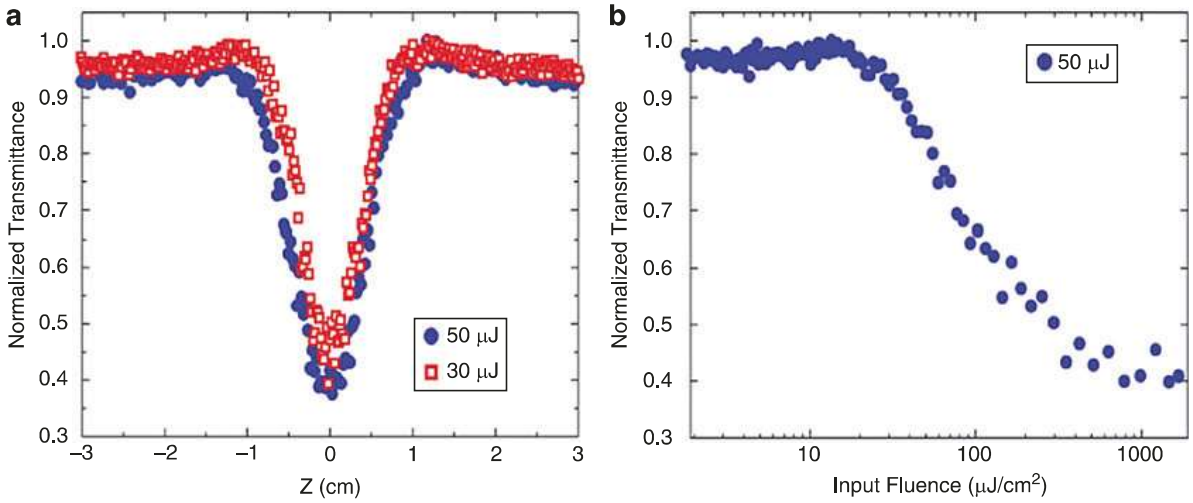

Nonlinear Optical Absorption and Induced Thermal Scattering Studies in Organic and Inorganic Nanostructures, Fig. 12 (**a**) Z-scan curves for nickel sulfide nanoparticles in 2-propanol and (**b**) the corresponding plot of optical transmission as a function of input fluence

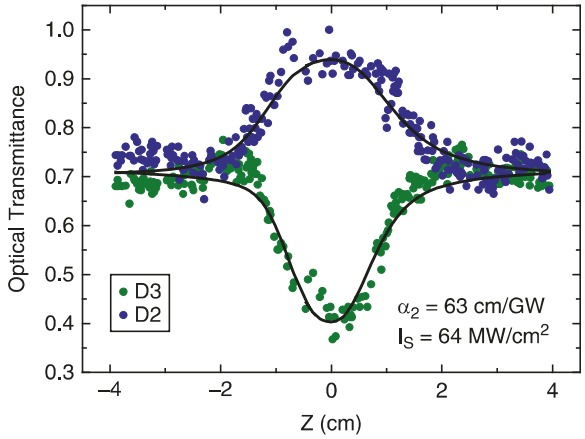

Nonlinear Optical Absorption and Induced Thermal Scattering Studies in Organic and Inorganic Nanostructures, Fig. 13 Z-scan curves of detector D3 (•) and D2 (•). While D3 measures the contribution of both nonlinear scattering and nonlinear absorption, D2 gives a measure of the intensity-dependent absorption alone

The UV–vis absorption spectrum for NiS_2 nanoparticles shows a strong absorption at ~554 nm (Fig. 14). Under 532-nm excitation, the nanoparticles are excited from the ground state (labeled "0") to a higher state (labeled "1") as shown in the *inset* in Fig. 14. As the intensity of the exciting laser pulse is increased to a maximum of 200 MW/cm^2, most of the nanoparticles occupy the excited state. As the ground state is bleached, the system becomes increasingly transparent to the incident laser pulse at 532 nm, resulting in a saturation of absorption and the consequent *Z*-scan curve.

The intensity-dependent absorption coefficient for a two-level system is given by [2]:

$$\alpha_{SA}(I) = \frac{\alpha_0}{1 + \frac{I}{I_s}} \tag{5}$$

where α_0 is the absorption coefficient, I is the intensity of the laser beam, and I_S the saturation intensity. This explains the upper curve in Fig. 13. The bottom curve can be understood in terms of simultaneous nonlinear intensity-dependent scattering that occurs due to energy transfer from nonradiative decay of excited states, as explained earlier in discussions of MWNT and Bi nanorod systems.

A complete description of the *Z*-scan experiment requires that both the saturable absorption and optical extinction due to nonlinear scattering be taken into account. Thus, in the similar lines of Venkatram et al. [18], we use the following equation describing these two concomitant processes:

$$\frac{dI}{dz} - \left[\alpha_0 + \alpha_2 I + \frac{\alpha_0}{1 + \frac{I}{I_s}}\right] I \tag{6}$$

N

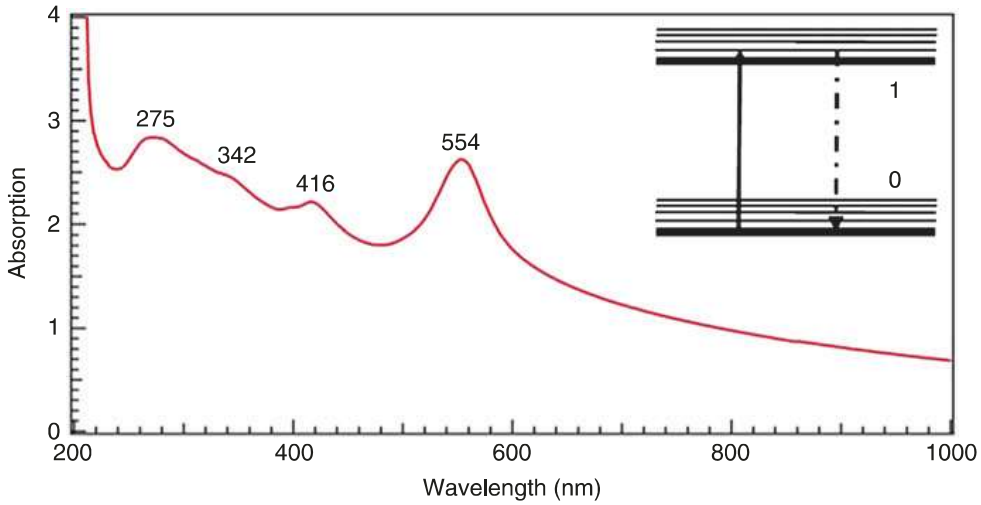

Nonlinear Optical Absorption and Induced Thermal Scattering Studies in Organic and Inorganic Nanostructures, Fig. 14 UV-Visible spectrum of NiS_2 nanoparticles in 2-propanol. *Inset* is a schematic of the excited manifold for saturable absorption as explained in the text

In the above equation, α_2 is the nonlinear scattering coefficient. The value of I_S and α_2 can be extracted from numerical fitting of data to this propagation. Here, the fourth-order Runge–Kutta method is used to solve the equation while finding the best fit for both parameters [6]. As mentioned earlier, the *Z*-scan curve of D2 is purely due to absorptive effects. The equation is first solved setting $\alpha_2 = 0$ so as to obtain a value for *IS* which in this case is 64 MW/cm^2. This value of *Is* is much smaller than the incident intensity at the focal point (at both 30 μJ and 50 μJ), eventually favoring the domination of nonlinear scattering following the absorption of a faction of the leading part of the incident pulse. Thereafter, the value of α_2 was obtained by using this value of I_S in the complete equation and finding the best fit to the Z-scan curve from detector D3. The nonlinear scattering coefficient, α_2, was found to be 63 cm/GW.

ZnO Nanostructures

Among the metal oxides, ZnO is a remarkable wide bandgap (3.37 eV in bulk) II–VI semiconductor. Its high exciton binding energy (60 meV) allows efficient exciton emission even at room temperature. As a consequence of its noncentrosymmetric crystal structure, ZnO is expected to have nonzero second-order susceptibility. Although many properties of bulk and nanostructured ZnO have been well studied, there is still a lack of understanding in the relationship between the density of defects, dopant level, synthesis conditions, and the observed optical and magnetic properties. In nanostructures, a fairly high surface state density significantly modifies or alters the chemical and physical properties, which can be reflected in optical measurements. NLO properties of different forms of pristine ZnO, such as single crystals, thin films, nanolayers, and nanowires, have been previously reported. It is also very important to understand the NLO properties of transition metal (TM)-doped ZnO nanostructures due to their ferromagnetic ordering at room temperature and importance in spintronic applications. An extensive study of NLO properties of TM-doped ZnO nanostructures can lead to a better understanding of the impact of surface states.

In earlier studies of the origin of ferromagnetism (FM) in pristine micro- and nanostructured ZnO, Podila et al. observed the changes in magnetic properties with varying crystallinity. They attributed the FM to the presence of surface states [8]. The presence of such surface states in pristine and Co-doped ZnO nanostructures (denoted as AP-CVD and AP-CoZnO) can be confirmed using the open aperture Z-scan. It is worth noting

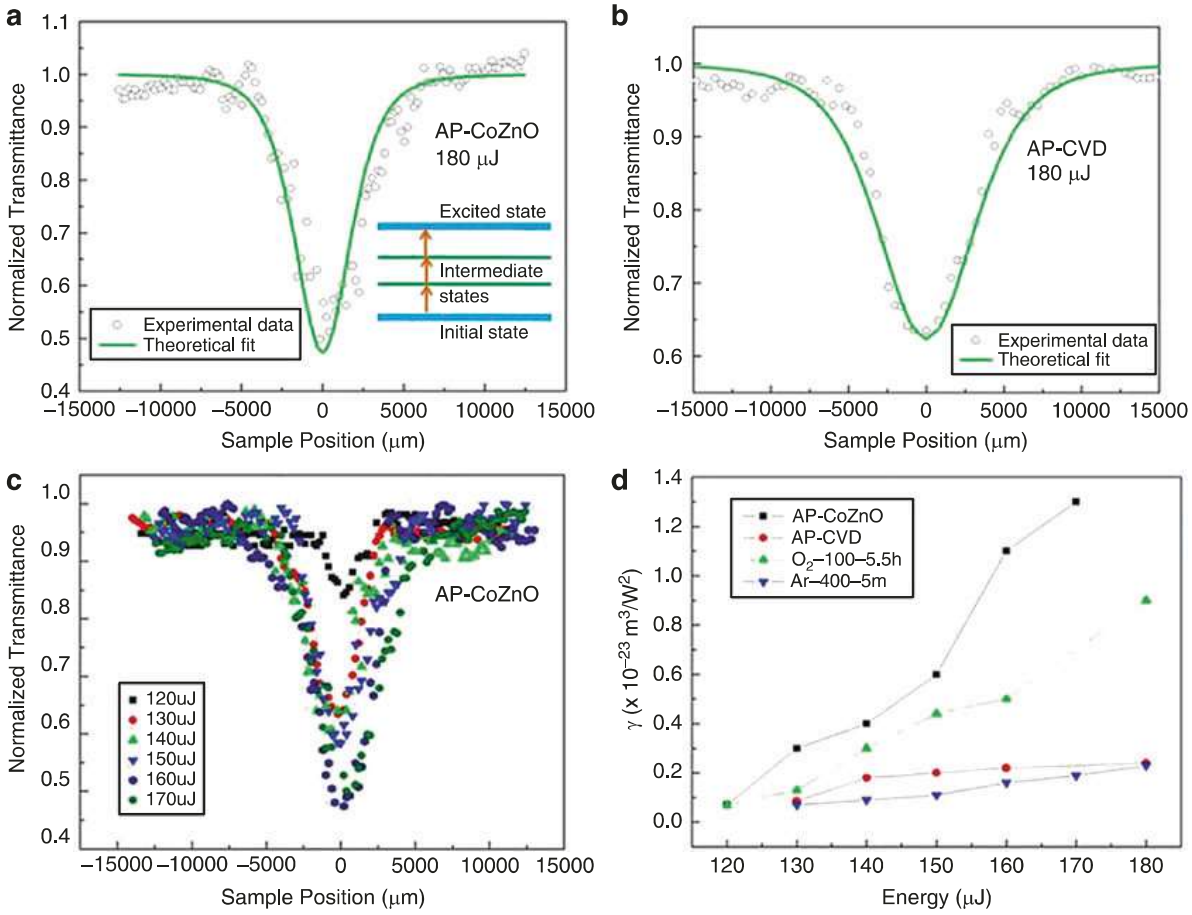

Nonlinear Optical Absorption and Induced Thermal Scattering Studies in Organic and Inorganic Nanostructures, Fig. 15 (**a**) Z-scan data for AP-CoZnO samples fitted to a three-photon absorption (*3PA*) equation. *Inset* is a schematic depicting effective 3PA. When the intermediate states are virtual, the effect is genuine 3PA, but when they are real, it is an effective 3PA arising mostly from excited state absorption. (**b**) Z-Scan data for pristine ZnO samples fitted to a 3PA equation. (**c**) Z-scan data for AP-CoZnO samples at different incident laser energies. (**d**) Variation of the 3PA coefficient (γ) as a function of the incident laser pulse energy for AP-CVD, AP-CoZnO, O_2-100-5.5 h and Ar-400-5 m samples

that, except when excited by ultrafast laser pulses, ΔT strongly depends on the excited state population density. In view of this, the nonlinear transmission of the ZnO samples was measured in the nanosecond excitation regime using linearly polarized 5-ns optical pulses from a Q-switched frequency-doubled Nd:YAG laser operating at 532 nm. The Z-scan data obtained for AP-CoZnO and AP-CVD samples (Fig. 15a, b, respectively) were found to be best-fit numerically by a three-photon absorption (3PA) process model. It is instructive to note that, compared to the 2PA process described in Eq. 7, the nonlinear absorption coefficient α in the presence of 3PA is given by

$$\alpha(I) = \alpha_o + \gamma I^2 \tag{7}$$

In the above equation, I is the intensity of the laser, α_o the unsaturated linear absorption coefficient, and γ the 3PA coefficient. The value of γ was obtained by fitting the Z-scan curve to the 3PA propagation equation, given by

$$\frac{dI}{dz} = -\alpha_o I - \gamma I^3 \tag{8}$$

with z' being the propagation distance within the sample.

The values of γ numerically obtained from the fits indicated that nonlinear absorption in the

present case arises not only from genuine 3PA but also from "effective" three-photon nonlinearity [1]. Such effective 3PA originates from sequential excited state absorption as shown in the inset of Fig. 15a. In the case of genuine three-photon absorption (3PA), where the transition states involved are virtual, the 3PA coefficient (γ) is a constant and is independent of the incident laser fluence. All genuine ground state absorption coefficients (such as 2PA or 3PA) are dependent on the ground state population N since the absorption coefficient is obtained by multiplying the corresponding absorption cross section (σ) by N. The absorption cross section is a microscopic parameter, independent of N that characterizes the average two-photon/three-photon absorbability per molecule. However, the change in γ will be evident only when there is a substantial change in the ground state population due to absorption. Therefore, if the absorptions are weak, then the coefficients can be considered to be almost constant, since there is a negligible change in N. Genuine 2PA and 3PA are usually very weak phenomena, and, hence, the corresponding coefficients can be considered as material constants at a given wavelength and concentration. But strong excited state absorptions (ESA) during an effective 3PA deplete the ground state population significantly so that the absorption coefficient is no longer a constant. Hence a change in γ with respect to the incident laser intensity can help confirm the presence of surface states in the forbidden gap of ZnO.

Both two-photon absorption and/or sequential absorption of two photons at 532 nm (2.33 eV; inset Fig. 15a) will result in a real terminal level which is above the lowest excitonic state that lies around 363 nm (3.4 eV) for ZnO, and another one-photon absorption to go from this level to the band edge. Figure 15c, d show the variation of γ for AP-CoZnO, AP-CVD, and AP-CVD samples annealed in O_2 (Ar) for 5.5 h (5 min) at 100 °C (400 °C)−O_2-100-5.5 h and Ar-400-5 m, respectively – as a function of incident laser energy. While γ remains almost constant with input energy in AP-CVD, there is a pronounced increase in γ with incident energy in AP-CoZnO and O_2-100-5.5 h samples. Moreover, the 3PA coefficient (and, hence, the optical limiting efficiency) for AP-CoZnO samples is obviously higher than that of pristine ZnO. These observations concur with the enhancement seen in the magnetic moment of AP-CoZnO and O_2-100-5.5 h samples and indicate the presence of enhanced surface state density due to Co atoms in the ZnO lattice. Thus, the increase of γ with the incident laser energy confirms effective 3 PA due to the existence of a wide range of surface states in AP-CoZnO and O_2-100-5.5 h samples. Furthermore, the lowest γ values and a constant trend with input fluence were observed for Ar-400-5 m samples indicating the absence of any surface states. An enhanced surface state density in AP-CoZnO due to Co doping results in stronger FM and better optical limiting compared to pristine ZnO nanostructures [19].

Conclusion

In the preceding sections, the reader is introduced to optical nonlinearities and given an overview of various methods used for nonlinear optical characterization with emphasis on the *Z*-scan technique. The chapter discusses in detail the NLO properties of various nanostructures, such as carbon nanotubes, bismuth nanorods, NiS_2 nanoparticles, and ZnO nanowires, studied using the Z-scan. In the case of MWNTs and Bi nanorods, nonlinear scattering is found to play a major role in determining the nonlinear transmission. The simultaneous onset of two different nonlinear processes (saturable absorption and nonlinear scattering) was observed in NiS_2 nanoparticles. In pristine and doped ZnO nanostructures, the intensity dependence of the 3PA coefficient could be used to confirm the presence of intermediate states. These studies indicate that organic as well as inorganic nanostructures are excellent candidates for nonlinear optical transmission with potential strategic applications, including optical power limiting.

References

1. Sutherland, R.L.: Handbook of Nonlinear Optics. Marcel Dekker, New York (1996)
2. Nalwa, H.S., Miyata, S.: Nonlinear Optics of Organic Molecules and Polymers, p. 841. CRC Press, BacoRato (1997)
3. Sheik-Bahae, M., Said, A.A., Wei, T.H., Hagan, D.J., Van Stryland, E.W.: Sensitive measurement of optical nonlinearities using a single beam. IEEE J. Quantum Electron. **26**, 760 (1990)
4. Tutt, L.W., Boggess, T.F.: A review of optical limiting mechanism and devices using organics, fullerenes, semiconductors and other materials. Prog. Quantum Electron **17**, 299 (1993)
5. Gu, B., Lou, K., Wang, H.T., Ji, W.: Dynamics of two-photon induces three-photon absorption in nanosecond, picosecond and femtosecond regimes. Opt. Lett. **35**, 3 (2010)
6. Rao, S.V., Srinivas, N.K.M.N., Rao, D.N.: Nonlinear absorption and excited state dynamics in Rhodamine B studies using Z-scan and degenerate four wave mixing techniques. Chem. Phys. Lett. **361**, 439 (2002)
7. Balu, M., Joel, H., David, H., Van Stryland, E.: White-light continuum Z-scan technique for nonlinear materials characterization. Opt. Express **12**(16), 3820–3826 (2004)
8. Podila, R., Queen, W., Nath, A., Fazzio, A., Schonalez, A., He, J., Dalpian, G., Skove, M.J., Hwu, S.J., Rao, A.M.: Origin of FM ordering in pristine micro- & nanostructured ZnO. Nano Lett. **10**, 1380 (2010)
9. Chin, K.C., Gohel, A., Elim, H.I., Chen, W., Ji, W., Chong, G.L., Sow, C.H., Wee, A.T.S.: Modified carbon nanotubes as broadband optical limiting nanomaterials. J. Mater. Res. **21**, 2758 (2006)
10. Pan, H., Chen, W., Feng, Y.P., Ji, W.: Optical limiting properties of metal nanowires. Appl. Phys. Lett. **88**, 223106 (2006)
11. Philip, R., Kumar, G.R., Sandhyarani, N., Pradeep, T.: Picosecond optical nonlinearity in monolayer protected gold, silver, and golf-silver alloy nanoclusters. Phys. Rev. B **62**, 13160 (2000)
12. Ganeev, R.A., Ryasnyansky, A.I., Redkorechev, V.I., Fostiropoulos, K., Prieb, G., Usmanov, T.: Variations of nonlinear optical characteristics of C60 thin films at 532 nm. **225**, 131 (2003)
13. Margulis, A.: Theoretical estimations of third-order optical nonlinearities for semiconducting carbon nanotubes. J. Phys. Condens. Matter **11**, 3065 (1999)
14. Joudrier, V., Bourdon, P., Hache, F., Flytzanis, C.: Nonlinear light scattering in a two-component medium: optical limiting application. Appl. Phys. B Lasers Opt. **67**, 627 (1998)
15. Black, M.R., Lin, Y.-M., Cronin, S.B., Rabin, O., Dresselhaus, M.S.: Infrared absorption in Bi nanowires resulting from quantum confinement. Phys. Rev. B **65**, 195417 (2002)
16. Sivaramakrishnan, S., Muthukumar, V.S., Reppert, J., Anija, M., Sivasankara Sai, S., Philip, R., Venkataramaniah, K., Kuthirummal, N., Rao, A.M.: Nonlinear optical scattering and absorption in Bi nanorod suspensions. Appl. Phys. Lett. **91**, 093104 (2007)
17. Muthukumar, V.S., Kiran, J.K., Reppert, J., Satyajit, R., Krishna, V., Nageshwar Rao, G., Siva Rama Krishnan, S., Siva Sankara Sai, S., Venkataramaniah, K., Rao, A.M.: Nonlinear optical transmission of surface modified NiS nanoparticles: saturation of absorption and optical limiting. NANO: Brief Rep. Rev. **3**, 161 (2008)
18. Venkatram, N., Sai Santosh Kumar, R., Narayana Rao, D.: Nonlinear absorption and scattering properties of CdS nanocrystals with its application as a potential optical limiter. J. Appl. Phys. **100**, 074309 (2006)
19. Podila, R., Anand, B., West, J.P., Philip, R., He, J., Skove, M., Hwu, S.J., Rao, A.M.: Evidence for surface states in pristine and Co-doped ZnO nanostructures: magnetization and nonlinear optical studies. Nanotechnology **22**, 095703 (2011)